 Bull. Chem. Soc. Jpn., 75, 899–908 (2002)

Accounts

Applications of Ultrafast Transient Infrared Spectroscopies

Todd A. Heimer and Edwin J. Heilweil*

Optical Technology Division, National Institute of Standards and Technology,
Mail Stop 8441, Gaithersburg, MD 20899-8441, USA

(Received November 21, 2001)

Broadband femtosecond and longer timescale mid-infrared and far-infrared (THz) probing techniques being explored at NIST using multi-element, mid-infrared focal plane arrays and solid-state THz generators/detectors are presented. Ultrafast infrared pulse generation, detection and pump-probe spectroscopy schemes are first reviewed in detail. These methods are used to examine transitory vibrational, chemical and electron transfer phenomena amenable to time-resolved infrared spectroscopy. Direct monitoring of electron transfer rates ($> 5\times10^{12}$ s) from dye sensitizers ($[Ru(dceb)(bpy)_2]^{+2}$ and $Ru(dcb)_2(NCS)_2$ derivatives) anchored to semiconductor solar-cell substrates (nanoparticle TiO_2, ZrO_2 and SnO_2 films) is accomplished by measuring increased mid-IR absorption originating from C=O groups and injected electrons in the substrate. Coherent control of CO-stretching vibrational overtone population distributions in liquid-phase metal-hexacarbonyl systems using deliberately chirped mid-IR excitation pulses has also been explored. Identification of molecular steric and diffusional properties involved in internal ring-closing reaction dynamics of ultraviolet (UV) photo-dissociated $(RCp)Mn(CO)_3$ systems in n-hexane will be presented. Terahertz spectroscopic methods and pulsed THz spectra of calf-thymus DNA, proteins and model dipeptides are also presented and their potential use for extracting bio-molecular functional dynamics discussed.

The application of ultrafast transient infrared (IR) spectroscopy to the study of chemical, biochemical and related physical phenomena has dramatically increased over the last decade. This surge of interest has largely been inspired by the increased availability of commercial, solid-state, table-top pulsed laser equipment and nonlinear frequency conversion methods for generating high power, broadly tunable infrared pulses in the near to mid-infrared wavelength regime (ca. 2 μm to 25 μm). Indeed, the accessibility and flexibility of these modern optical systems has far exceeded the expectations of many researchers working in this field. Early methodologies for generating ultrafast IR pulses used simple multi-pass optical parametric amplifiers[1] or visible difference frequency mixing techniques[2] to access the mid-IR spectral region. Dynamical measurements of vibrational energy flow within solute and adsorbate species begun in the late 1970's[3] has given way to highly sophisticated ultrafast methods,[4] studies of ultrafast molecular reaction mechanisms,[5] energy transfer within short-chain amino acids,[6] at surfaces,[7,8] and in liquids[9,10] and solids,[11] to name a few examples.

Early ultrafast transient infrared measurements were typically performed using identical frequency picosecond infrared pulses for both pumping and probing a vibrational mode of condensed-phase molecules.[12] In this scenario, an intense, narrow-band tunable infrared pump pulse excites population from the $v = 0$ to $v = 1$ level of a molecular vibration (producing increased sample transmission) and a weaker probe pulse interrogates the recovery of ground state absorption to yield the $v = 1$ population relaxation time (T_1 lifetime). These simple "single color" measurements were quickly superceded by "two color" techniques since it was recognized that monitoring the transient infrared spectrum as a function of time yields much more detailed information about the system dynamics. For example, detection of mode-specific vibrational solute-to-solvent energy transfer[13] or the generation of new transient reaction intermediates[14] necessarily dictates that a tunable infrared probe pulse be used to observe new spectral features removed in frequency from the parent molecular absorptions. However, using tunable, narrow-band probe pulses to obtain broadband spectra involves the arduous task of taking frequency-scanned spectra with single element detectors at multiple pump-probe time delays. This generic approach suffered from extended data acquisition times for low repetition rate laser systems and potential long-term drift problems that potentially distorted the spectral intensity information.

To circumvent these difficulties, broadband infrared detection using multi-channel arrays was employed by our group[15,16,17] and others.[18,19] In many respects, this approach is complementary to the accepted technique for performing ultraviolet-visible transient absorption spectroscopy. By generating broadband mid-infrared probe pulses a few picoseconds or less in duration and detecting a portion of an infrared spectral re-

gion for each laser pulse, data acquisition rates are vastly enhanced and system stability issues are diminished. It should also be pointed out that picosecond or femtosecond broadband probe pulses can be used to detect narrow-band transient absorption features as long as the transient absorber has lived on the order of the coherence (T_2) lifetime of the interrogated state.[20] These typically narrow-band features (3 cm^{-1} to 15 cm^{-1} FWHM) are spectrally resolved by an up-converter crystal (with CCD detection) or through the spectrograph resolution independent of the inherent time-bandwidth characteristics of the probe pulse. Demonstrations of the general broadband IR detection approach were first made using nonlinear IR frequency down and up-conversion with visible spectrograph-CCD detection.[15,16] With Defense Department declassification and increased commercial availability of infrared focal-plane arrays for mid-infrared imaging use, direct broadband infrared spectroscopic detection covering the 1 μm to12 μm range is now practical.[21]

We first describe the state-of-the-art in using ultrafast picosecond and femtosecond lasers to generate tunable, broadband mid-infrared pulses for time-resolved spectroscopic applications. Methods developed for acquiring transient IR spectra using multi-element array technologies is presented. After discussing these techniques, selected studies performed at NIST using these broadband techniques are reviewed. In these exploratory cases, transient infrared spectroscopy yielded new insight into previously unknown transient species that exist during molecular chemical reactions, helped develop methods for controlling population in molecular vibration overtone states, and revealed injection rates of electrons transferred from adsorbed ruthenium-based dyes into conducting TiO_2 substrates.[22] It is hoped that an overview of these different examples and new ventures into the far-infrared (or terahertz = THz) spectral region will inspire and promote various extensions of the broadband ultrafast IR technique for future research endeavors and spectroscopic applications.

Experimental

The production of ultrafast mid-IR pulses begins with a fixed-frequency laser oscillator that is pulse amplified from nanojoule energies to microjoule (μJ) and millijoule (mJ) levels. The laser systems used include a Nd^{3+}:YAG 80 MHz picosecond oscillator (100 ps, 1.064 micron) and a Ti:Sapphire 35 fs oscillator followed by multiple-pass or regenerative amplifiers. These amplified pulses are subsequently frequency-shifted or beat against another pulse (by frequency down-conversion steps) in an appropriate nonlinear crystal to reach the mid-IR range. Various frequency-shifting techniques include difference frequency generation between two synchronously pumped tunable dye lasers or optical parametric amplification (OPA) of a weak infrared continuum which provides narrow-bandwidth tunability in the mid-IR region at moderate power levels ($<$ 20 μJ/pulse). Difference frequency mixing of amplified tunable visible dye oscillators beat against a fixed frequency pulse (e. g., the 532 nm second harmonic of the Nd^{3+}:YAG) in $LiIO_3$ crystals enabled generation of independently tunable IR pump and probe pulses.[2] The above approaches produced tunable 1 ps to 20 ps pulses with relatively narrow (3 cm^{-1} to 10 cm^{-1} FWHM) spectral bandwidths appropriate for single-frequency "point-by-point" spectral interrogation of condensed-phase systems. For reference, a combined schematic for the 80 MHz YAG and Ti:Sapphire based laser systems used at NIST with mixing optics and crystals capable of providing a tunable (UV to IR) pump and broadband IR probe is shown in Fig. 1.

Modifications to the above laser systems and frequency down-converting schemes are readily performed to generate broadband

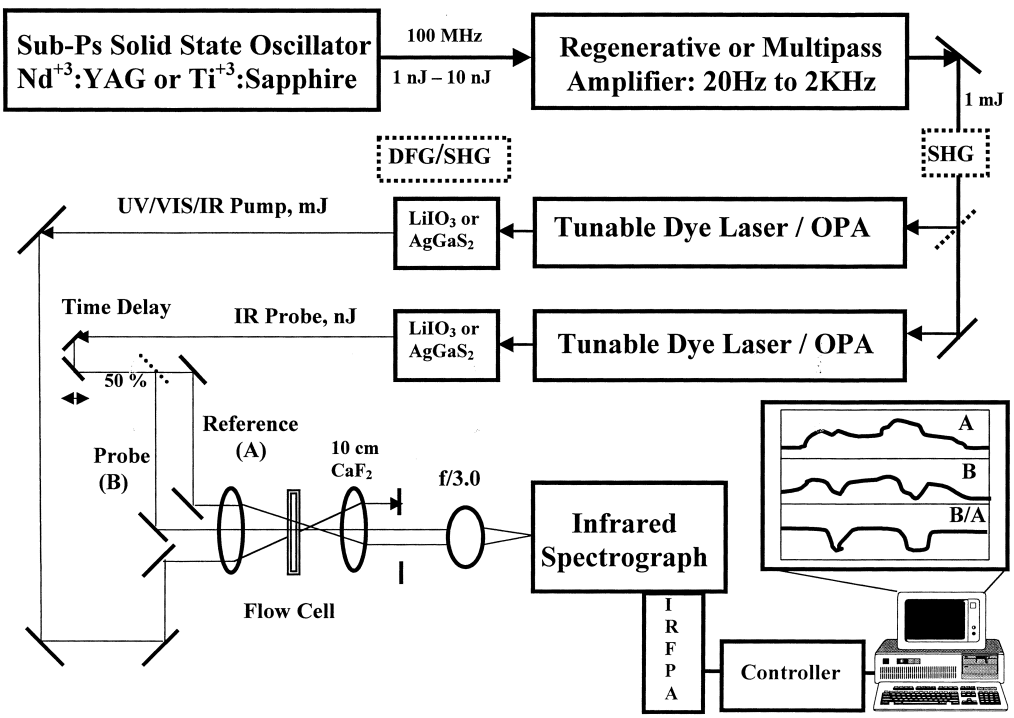

Fig. 1. Transient broadband infrared system schematic using IR Focal Plane Array (IRFPA) dual track detection.

IR output. For example, synchronously-pumped picosecond visible or near-IR dye oscillators deliberately run without intracavity tuning elements permit the lasers to run broadband with output center frequency dictated by the dye gain spectrum.[15] Sub-picosecond dye laser pulses can also be fiber frequency chirped, amplified (to $<$ 1 mJ) in three-stage dye amplifiers, grating compressed to $<$ 150 fs pulse duration and then mixed against a 5 ps to 10 ps, 300 μJ dye pulses in $LiIO_3$ to yield 150 fs to 200 fs FWHM broadband (200 cm^{-1} to 300 cm^{-1} FWHM) IR output.[22] When beat against the second harmonic of the Nd:YAG amplifier or another amplified picosecond (i. e., narrow-band) dye laser in $LiIO_3$ or $AgGaS_2$, this approach yields pulses in the 3 μm to 10 μm spectral region of up to several hundred wavenumbers bandwidth (FWHM). Difference frequency generation between a broadband seed pulse and narrow-band pump pulse ensures that the generated broadband IR pulse experiences minimal temporal dispersion or jitter while traversing the nonlinear crystal. Dye-based broadband sources (deliberately run without intracavity seeding) are inherently spectrally noisy and require shot-to-shot normalization and averaging during data collection (see below). However, there is no inherent reason why this general method cannot be extended to longer wavelengths for probing in the molecular "finger print" (6 μm to 12 μm) region. To date, most investigations of organic C=O stretching modes in the 6–7 μm range have been conducted[6,19,23,24] but little if any known transient IR work has been performed in the 8 μm and longer wavelength range.

The other laser system employed for our work is based on femtosecond Ti:sapphire oscillators (80 MHz, pulse duration $<$50 fs FWHM, ~800 nm, 0.35 Watt average power) and kilohertz multipass amplifier capable of delivering approximately 1 Watt of output power used as pulsed sources. This system possesses the desirable characteristics of delivering ultrafast (but only slightly tunable) pulses which maintain their inherent near transform-limited broadband characteristics ($>$ 100 cm^{-1} FWHM) and high repetition rates for rapid data collection and signal averaging. Tunable frequency down-conversion employs a BBO-based (β-Barium Borate) OPA (with multiple BBO passes) that "split" a nominally 800 nm, amplified Ti:sapphire input pulse into two longer-wavelength pulses (signal and idler tunable between 1.1 μm to 2.9 μm). These pulses are subsequently co-propagated and temporally recombined in a down-converting mixing crystal (e. g., Type I $AgGaS_2$) to produce tunable, relatively broad-bandwidth ($>$ 150 cm^{-1} FWHM, $>$ 1.8 μm) mid-IR probing pulses. The salient features of producing IR pulses in this fashion are straight-forward tuning of the solid-state OPA to cover the desired mid-IR spectral range (accessible between 2 μm to 12 μm), natural short pulse duration for time-resolved measurements, the inherent energy stability (a few percent rms amplitude noise) and smooth nearly transform-limited broadband spectral output. Generated IR pulses containing a few microjoules of energy are more than sufficient for subsequent up-conversion with CCD detection or direct IR focal plane array detection schemes discussed in the next section.

Broadband Up-Conversion with CCD Detection. One of the first known demonstrations of broadband IR probe pulse generation and detection used a 30 picosecond Nd^{3+}:YAG laser system with two synchronously pumped, amplified dye lasers and dual solid-state $LiIO_3$ down and up-converting crystals. Broadband detection was accomplished with a double-grating visible spectrograph and visible Si-CCD detector.[15] In this configuration, IR pulses of about 20 ps FWHM duration with bandwidths on the order of 100 cm^{-1} to 200 cm^{-1} FWHM were generated and detected in the 4.8 μm to 5.0 μm range. These pulses were produced by down-conversion mixing of the amplified, broadband Rhodamine-B or Rhodamine 610 dye lasers against the second harmonic (SHG, 532 nm) output of the amplified Nd^{3+}:YAG laser. Slightly broader bandwidth pulses were actually generated because phase-matched angle tuning of the up-converting crystal produced broader spectral output of the detected up-converted spectrum. It should be noted that this approach is capable of producing two independently tunable pump (UV-vis or IR) and broadband probe pulses with approximately 20 ps instrumental time resolution.

Transient IR spectra were typically obtained by splitting the broadband IR pulse into two energy balanced beams ("reference" and "probe") which were up-converted after the sample by two independently timed and spatially overlapped Nd:YAG SHG pulses in a single $LiIO_3$ crystal.[14] These up-converted pulses were dispersed by a f/4.0 double spectrograph (1200 g/mm holographic gratings) and imaged onto the focal plane of a 378×512 element Si:CCD array to yield two parallel spectral tracks (ca. 10 pixels high separated by 1 mm to 2 mm). The excitation pulse (e. g., a UV pulse at 289 nm generated via SHG of one of the dye laser pulses) was overlapped with the IR probe beam in a flowing liquid sample cell (ca. 1 mm pathlength, 0.1 mm beam diameter) placed between two 10 cm focal length matched CaF_2 lenses. Alternate on-off chopping of the pump beam was employed to monitor probe pulse spectral changes during the data collection time. This approach greatly reduced long-term drift of an acquired spectral baseline. Software was developed to collect the vertically integrated spectra and average the data to obtain a difference spectrum. By obtaining the ratio of the probe versus reference spectrum on each laser shot, baseline noise for 4000 averaged shots (about 10 minute collection time at 20 Hz) was typically measured to be about 0.25% (1σ standard deviation case A, $k = 1$). The system exhibited about 4 cm^{-1} FWHM spectral resolution (2.8 cm^{-1}/pixel dispersion) with a spectral window of about 200 cm^{-1} in the 5 μm wavelength region. We note that under these collection conditions, one attains an effective "single wavelength" data acquisition repetition rate of 1.4 kHz with this system.

Spectral resolution and transient IR tests of this instrument were conducted using metal-carbonyl species dissolved in *n*-hexane. These systems were studied in part because they typically exhibit strongly absorbing (peak molar extinction coefficient of the order 10^4 L/mol-cm) and narrow CO-stretching features (ca. 3 cm^{-1} FWHM in *n*-hexane) in the 1800 cm^{-1} to 2100 cm^{-1} region.[24] A variety of experiments using the above picosecond apparatus and a shorter time-resolution, sub-picosecond (fiber chirped-amplified-compressed) synchronously-pumped dual-dye laser system successfully monitored metal-carbonyl vibrational energy transfer[25] and reaction dynamics[26] for several systems in room-temperature solution. This set of experiments revealed vibrationally "hot" photoproducts,[23] new transient metal-carbonyl solvated species[27] and helped extract their ultrafast reaction kinetics by this inherently straightforward broadband probing approach.

Direct Broadband Detection Using Infrared Focal Plane Arrays. After performing multiple experiments with the CCD up-conversion technique described above, it became apparent that several improvements could be made to the apparatus if the nonlinear up-converting step was eliminated. Most importantly, it was determined that the detectable up-conversion bandwidth was generally strongly dependent on the crystal acceptance angle and input focusing parameters. Because this angle is frequency and

crystal length dependent, severe reduction of the detected generator output bandwidth was observed at wavelengths greater than 3 μm to 5 μm. For example, when performing electron injection studies near 6 μm using a 5 mm long $AgGaS_2$ crystal, usable bandwidth windows of only 20 cm^{-1} to 30 cm^{-1} were obtained.[22] Additionally, it was felt that improved signal-to-noise difference spectra (over CCD detection) could be attained if direct, IR spectrograph with multi-channel infrared detection were possible. These alterations were potentially achievable if an infrared focal plane array detector (acronym IRFPA, or dual linear arrays on the same substrate) were used. Otherwise, the approach for generating two probe and reference beams (for single shot normalization) would be the same as for CCD detection except an IR spectrograph and beam delivery optics are employed.

Exploration of IRFPA sources in early 1994 revealed that several US Defense Department contract manufacturers produced InSb (1 μm to 5.5 μm) and HgCdTe (or MCT, for 2 μm to 12 μm) 256×256 and smaller arrays (< 65,536 total pixels on 30 μm centers) with built-in multiplexers for imaging projects.[21] One requirement for pulsed spectroscopic applications is that an array be run in "snapshot" rather than normal imaging strobing read-out format. This characteristic is necessary because a constantly strobing read-out device is incapable of capturing a single ultrafast laser pulse spectrum over the width of the array. For a snapshot array, all diode electron capacitive wells accept charge during the same integration period. After pulse integration (typically ca. 10 μsec), the array is subsequently read out (using one or more analog outputs) by a clocking sequence and an image reconstructed from the analog-amplified and digitized chip output. Customized software was developed to vertically integrate the digitized spectral image to extract the two track spectra, and to perform normalization, averaging, and automated data collection with user display functions. Many of the snapshot IRFPAs available at that time could support 20 Hz to 50 Hz frame rates by using dual outputs for the formats described above. We elected to use two 256×256, 30 μm pixel pitch InSb (sensitive from 0.5 μm to 5.5 μm) and HgCdTe (sensitive from 3 μm to 12 μm) arrays produced by the same manufacturer (Santa Barbara Research Center)[28] and bonded to the same CD-585 dual output (maximum 1 MHz clock rate) multiplexer readout. These IRFPAs were installed in two interchangeable camera dewars (cooled by LN_2 at 77 K) so that the entire near to mid-IR (1 μm to 12 μm) wavelength range could be covered using the same controller, readout electronics, image capture board and custom software.

Currently produced 2-dimensional IRFPA devices, similar to those described above, use multiple image windowing or have up to four video outputs to produce higher frame rates (reaching several kHz) and are now available for related spectroscopic applications. New IRFPA detector arrays are constantly being designed (now with up to 2048×2048 HgCdTe pixel formats) for astronomical imaging which could also be employed for ultrafast IR spectroscopy. However, it should be noted that while these devices would potentially advance ultrafast IR spectroscopic investigations, they are still difficult and extremely expensive to acquire. The challenge is to find readily available sources for these components from manufacturers interested in spectroscopic versus imaging capabilities. It should be mentioned that there are only a few sources for custom single chips composed of dual linear multiplexed IRFPA devices that would be best suited for dual-track, shot-to-shot normalization for spectroscopic users. Single linear arrays have been produced with interleaved InSb and HgCdTe elements to enable complete mid-IR coverage. Linear 32-element HgCdTe arrays (50 μm wide by 1 mm high pixels with individual external pre-amplifier, sample-and-hold to parallel ADC circuits capable of very rapid read-out rates) without multiplexers are being used for broadband IR detection in conjunction with stable Ti^{3+}:sapphire kHz laser systems.[6,21] However, this approach reduces broadband wavelength coverage and spectral resolution because of the limited array and pixel size. A proposed advanced and potentially more versatile IRFPA design for mid-IR spectroscopy would incorporate two parallel 1024 element linear interleaved InSb/HgCdTe arrays manufactured with multiplexed read-outs on the same substrate. This format would enable dual track normalization for unstable pulse output and provide extremely wide-band coverage for general-purpose use.

Examples of time-resolved studies using the InSb and HgCdTe arrays described above will be presented in the next section. Because this method extracts small difference signals riding on top of large-valued spectral background counts, it was typically found that under nearly identical optical configurations for the CCD and IRFPA detector schemes, similar signal-to-noise spectra resulted. Apparently TE or LN_2 cooled CCD's with their inherently low but stable background count rates and high quantum efficiencies are optimal for extracting small visible signals on large spectral backgrounds. The IRFPAs, on the other hand, are still reasonably high quantum efficiency detectors (the QE is about 0.8 for InSb near 5 μm) but are constantly flooded with black-body background radiation making constant background subtractions difficult and adding error to extracted difference spectra. In practice, the advantage of detecting the entire broadband probe pulse bandwidth by using an appropriately chosen spectrograph and IRFPA with optimized spectral dispersion is preferential to the more complicated optical arrangement and limited detected spectral bandwidth of the visible spectrograph/CCD approach.

Applications of Broadband Infrared Spectroscopy

We discuss and review studies conducted using broadband probe pulse generation and detection methods described above. The examples presented were chosen to provide the reader with a synopsis of the techniques and state-of-the-art performance of the tested array technologies. It is anticipated that these examples will generate an appreciation for the methods employed to extract detailed mechanistic and kinetic information about a variety of chemical, biochemical and physical processes which occur in many research and applications areas.

Primary Electron Transfer Dynamics of Dye-Sensitized Semiconductor Solar Cell Devices. We discuss the use of broadband ultrafast infrared spectroscopy as a tool for monitoring electron transfer rates in dye-sensitized solar cell applications. Systems composed of Ru-bipyridine derivatives chemisorbed onto nanoparticle TiO_2 thin films exhibit highly efficient electron transfer to the substrate after photoexcitation of the adsorbed dye.[29] When dye-impregnated films are sandwiched between transparent electrodes (e. g., tin-oxide) and a redox couple electrolyte (typically I_2/I^- in propylene carbonate), these devices have been shown to produce currents with solar cell conversion efficiencies up to 10% and up to 80% absorbed photon to current ratio under monochromatic irradiation.[30] Because of the simplicity, reduced cost and potentially

high efficiency of these solar cells compared to conventional silicon-based cells, much recent effort has been expended to optimize and understand the fundamental electron transfer mechanisms responsible for improving these devices.

In early studies, transient ultraviolet and visible spectroscopies were employed to monitor the electron transfer rate from the adsorbed dye to the underlying substrate. Time-dependent emission or absorption measurements of the sensitizer (for dyes in solution or on ZnO_2 and TiO_2) and near-infrared absorption signals from injected electrons were measured.[30] Electron injection times ranging from picoseconds to several nanoseconds were obtained so it was felt that some of these kinetic rates could be affected by dye excited state interference or other intervening mechanistic processes. To eliminate these possibilities, investigations were initiated to determine whether transient broadband infrared spectroscopy would be sensitive to electrons directly injected into the nanoparticle semiconductor substrates and if vibrational modes of coordinated dye ligands could be used to monitor electrons transferring to the substrate.

We first employed picosecond time-resolved IR spectroscopy in the 6 μm spectral region to study the vibrational and electron dynamics of $[Ru(4,4'\text{-}(COOCH_2CH_3)_2\text{-}2,2'\text{-bipyridine})\text{-}(2,2'\text{-bipyridine})_2]^{2+}$ and $[Ru(4,4'\text{-}(COOCH_2CH_3)_2\text{-}2,2'\text{-bipyridine})(4,4'\text{-}(CH_3)_2\text{ -}2,2'\text{-bipyridine})_2]^{2+}$ in room temperature dichloromethane (DCM) solution and anchored to nanostructured thin films of TiO_2 and ZrO_2.[29] Visible excitation of the dyes reveals a red-shift of the CO-stretching mode (1731 cm^{-1}) of the ester groups for the free molecules in solution (see Fig. 2) and similar spectral changes when attached to insulating ZrO_2 substrates. However, for these molecules attached to TiO_2 semiconductor films, an extremely broad transient absorption throughout the mid-infrared and without any identifiable spectral features is observed. Our group and others[31,32] now attribute this broad signature to excited state absorption of electrons directly injected into the TiO_2 semiconductor substrate. Initial attempts to time resolve the appearance of injected electrons was unsuccessful because the rise-time of this absorption signal followed the instrumental cross-correlation between the visible and infrared pulses but a lower limit for the injection rate of ca. 5×10^{10} s^{-1} was deduced from this study. Subsequent investigations using the related non-ionic dyes $Ru(4,4'\text{-}(COOH)_2\text{-}2,2'\text{-bipyridine})_2(NCS)_2$ (**IV**) and $Ru(5,5'\text{-}(COOH)_2\text{-}2,2'\text{-bipyridine})_2(NCS)_2$ (**V**) covalently bound to TiO_2 were undertaken using higher time-resolution (350 fs FWHM VIS-IR cross-correlation). Again, an instrumentally determined response was measured for both species indicating the injection time is $<$ 350 fs (or 3×10^{12} s^{-1}) and that perhaps injection rates for other dyes could exceed this value.[29]

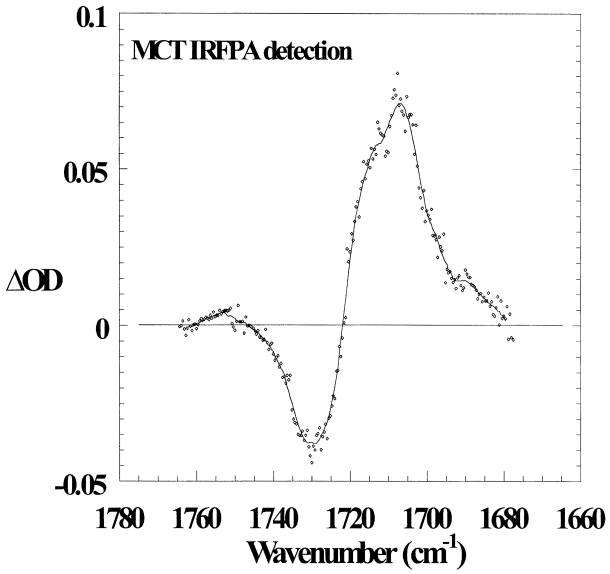

Fig. 2. Transient IR difference spectrum of $[Ru(dceb)\text{-}(bpy)_2]^{2+}$ in dichloromethane at room temperature 35 picoseconds after 532 nm excitation showing the parent CO-stretch bleach and red-shifted excited state absorption. The data points were obtained by direct broadband detection with a HgCdTe (MCT) 256 × 256 focal plane array system.

Ultrafast injection of carriers into the TiO_2 substrate suggests that overall cell efficiency is not limited by this process but by intervening transfer mechanisms (e. g., trapped state populations reducing quantum yield) or longer timescale electron-dye recombination rates (typically taking microseconds). For example, it was found that the absorbed photon to current efficiency (APCE) is considerably reduced for **V** compared to **IV** under identical cell conditions.[28,33] While **V** has a 350 mV lower electrochemical reduction potential than **IV** (and hence a red-shifted absorption spectrum), it is unclear why the redder absorbing dye (**V**) does not inject as efficiently.[32] Recent visible excitation with broadband UV-vis nanosecond probe experiments for the above dyes on TiO_2 and ZrO_2 suggest that injection only occurs on TiO_2 but the yield for **V** is lower than that for **IV** (exhibiting larger parent bleach and transient ligand or injected electron features).[32] This corroborates the previously mentioned transient IR measurement that also gave approximately one-half IR signal amplitude for **V** versus **IV**.[28] Recent transient UV-vis and APCE measurements for these same dyes anchored to nanostructured SnO_2 films (having 400 mV lower redox potential than TiO_2) indicate that **IV** and **V** inject with nearly equal and enhanced total efficiencies (about 45%) across the entire dye absorption band.[34] Perhaps both dyes are better matched to the SnO_2 bandgap and inject with higher quantum yield under these conditions. Continued broadband transient IR and UV-vis studies for these and related dye systems are clearly warranted to better understand the electron transfer mechanisms and rates for these important solar energy converters.

Vibrational Coherent Control with Chirped Picosecond Infrared Excitation.[35] Investigations of "vibrational coherent control" of molecular vibrational populations are now attainable with specifically tailored high power, chirped infrared ultrafast pulses. Controlling the phase and amplitude of an infrared excitation pulse that is properly tuned to adiabatically sweep population up a molecular vibrational manifold has been theoretically shown to produce population in specific overtone states.[36] By choosing pulse properties for coherently exciting vibrational population above a bond dissociation energy, for example, it may be possible to "control" the dissociation process and hence improve chemical reaction yields over

conventional thermally activated processes. Ultrafast (picosecond or shorter pulsewidths) chirped excitation naturally spans multiple anharmonic shifts (allowing access to higher energy vibrational states) as well as circumventing intrinsic population relaxation mechanisms. Broadband infrared probing is also ideal for monitoring population distributions as a function of time after coherent absorption of the excitation pump pulse.

We elected to study coherent up-pumping dynamics in solution-phase metal-hexacarbonyl systems because of their strong vibrational infrared absorption cross-sections, relatively simple ground-state spectra and small (ca. 15 cm^{-1}) anharmonic hot-band shifts. It was felt that these systems are ideal candidates to demonstrate that population control could be achieved for polyatomic species in solution because the excited state population lifetimes (T_1) were already known to be long-lived[14,22,24,25,37] and the coherence lifetimes for lower-lying states are also relatively long ($T_2 > 4$ ps). The first systematic investigation was conducted on the triply-degenerate CO-stretch T_{1u} mode ($v = 0 \rightarrow 1$ at 1986 cm^{-1}) of $W(CO)_6$ in *n*-hexane solution at room temperature.[38] It was known from previous work that the CO-stretch ($v = 1$) state has a T_1 lifetime of ca. 140 ps and that the system in n-hexane exhibits narrow (ca. 3 cm^{-1} FWHM) features.[14] Initial studies which used non-chirped, difference-frequency generated (near transform-limited) 2 picosecond, < 10 μJ pump pulses tuned across the $v = 0 \rightarrow 1$ absorption feature revealed that population distributions spanning up to the $v = 3$ overtone state could be altered by choice of center frequency. Generation of only CO ($v = 1$) population was achieved when the pump pulse was tuned and overlapped with the high frequency side of the 1986 cm^{-1} absorption feature. However, up to $v = 3$ excitation with nearly equal $v = 1$ and $v = 2$ populations (saturation) was achieved by tuning the pump pulse center frequency to the low frequency side of the same feature. Concomitant excited overtone state T_1 relaxation times were also deduced from the transient spectra, producing a monotonic lifetime reduction as one ascends the manifold.[38]

More advanced tests of vibrational "coherent control" theory were conducted by using deliberately chirped picosecond excitation pulses.[35] By deliberately mixing positively or negatively chirped 2 picosecond visible pulses (near 589 nm) with much longer, narrowband dye laser pulses (8 ps FWHM at 650 nm) in $LiIO_3$ crystals, one generates chirped IR pulses which experience negligible group velocity delay distortion. The sign of the chirp was produced by either passing a sub-picosecond dye pulse through a short length of optical fiber (red-to-blue or positive chirp) or by deliberately stretching a two-pass grating compressor to invert the phase (blue-to-red or negative chirp). Actual pulse chirp rates (ca. 10 cm^{-1}/ps) and signs were deduced from time versus directly obtained IR spectrum (via a spectrograph and InSb IR focal plane detector) datasets that were analyzed by the FROG (Frequency Resolved Optical Gating) iterative fitting algorithm.[39]

Results for up-pumping $W(CO)_6$ with chirped pulse excitation were compared to excitation of the T_{1u} manifold using transform-limited pulses with center frequencies all tuned to the peak vibrational mode absorption frequency. Fig. 3 shows transient broadband absorption spectra taken at 40 ps time delay for the three different pulse types. As depicted, one readily

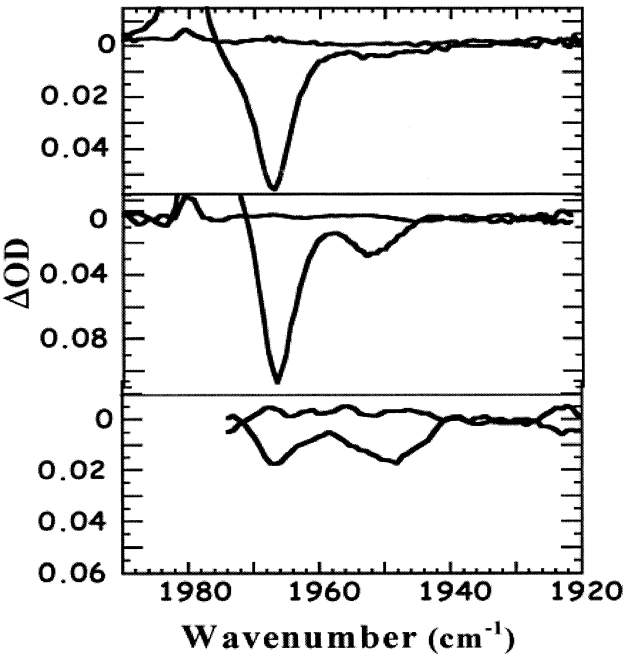

Fig. 3. Transient infrared spectra obtained at 40 ps time delay for $W(CO)_6$ in room temperature *n*-hexane using (top) positively chirped, (middle) no chirp and (bottom) negatively chirped 2 ps IR excitation pulses centered at 1983 cm^{-1}. Baseline noise (no pump pulse) is indicated at 0 ΔOD for each panel and induced absorptions point downward. Note the suppression of $v = 1$ signal at 1963 cm^{-1} and increase in $v = 2 \rightarrow 3$ excited state absorption near 1950 cm^{-1} when using negative chirp excitation (bottom panel).

observes that the relative population amplitudes in the CO-stretch $v = 1$ (at 1970 cm^{-1}) and $v = 2$ (at 1955 cm^{-1}) levels are strongly affected by the chirp of the excitation pulse. Excitation with negatively chirped pulses and ten times lower pump pulse energy was found to produce higher level populations than using non-chirped excitation. This general trend was confirmed by multi-level coherent up-pumping modeling using excitation pulse properties measured independently by the FROG technique.[39]

An attempt was made to extend the above study to excitation of higher overtone levels by using broader bandwidth femtosecond infrared excitation. Pulses generated by a tunable femtosecond mid-IR OPA (810 nm, 50 fs, 450 μJ 1 kHz input pulses) were analyzed by sum frequency cross-correlation (using a fraction of the OPA pulses and 50 fs 800 nm gating pulses) at the input surface of a *z*-cut quartz flat. Approximately 2 microjoule, 5 micron pulses were found to be slightly negatively chirped with an approximate pulse duration of 200 fs FWHM and 180 cm^{-1} FWHM bandwidth. The DFG output beam was propagated to the same experimental apparatus described earlier[35] for performing up-pumping excitation except that ca. 10% of the beam was split off with a 1 cm thick CaF_2 flat to generate a delayed set of probe and reference pulses. Using the significantly larger bandwidth and shorter IR pulse durations, one might expect to up-pump vibrational population into much higher overtone levels than $v = 3$ (as was observed

with picosecond IR pulses). However, only population in $v = 1$ was produced when using these excitation pulses (about 5% population was transferred from $v = 0$ to $v = 1$). A sequence of delayed transient spectra indicates that the $v = 1$ population exhibits the expected $T_1 = 110$ ps lifetime for $W(CO)_6$ in *n*-hexane so the sample and probing conditions were proper for detecting $v = 2$ and higher overtone populations. It remains to be explored when using the measured IR pulse parameters in our adiabatic coherent pumping model why excitation of only the $v = 1$ level is observed. One possibility is that the system was pumped in the extremely high Rabi limit, and with T_2 being a few picosconds in duration (i. e., much longer than the pulse duration), overtone excitation is not favored and only $v = 1$ excitation is produced under these conditions.

Theoretically predicted chirped-pulse excitation on the up-pumping dynamics of $W(CO)_6$ and related theories for diatomic rotational population distributions in the gas phase[40] suggest that overtone population distributions can be "controlled" with carefully generated chirped IR pulses. It still remains to be seen if deliberately chirped broadband IR femtosecond and picosecond pulses with inherently larger bandwidths and varying chirp rates can produce pure populations in specific vibrational overtones that lead to chemically interesting bond-breaking phenomena and ground state reactions.[41]

Ultraviolet Photochemistry: Self-Association Reactions of Species $MnCpR(CO)_3$ in Solution.[42] High quantum yield photochemical reactions of condensed-phase species may become useful for future optical applications such as molecular switches, optical limiters and read-write data storage media. Towards these ends, much research has been conducted on novel nonlinear chemical-based materials such as conducting polymers and metal-organic species. Monitoring the early time-dependent processes of these photochemical reactions is key towards understanding the fundamental mechanisms and rates which control the outcome of these reactions and could lead to improved speed and efficiencies of devices.

To investigate prototypical reaction processes, studies of $Mn(CO)_3CpR$ systems (Cp = cyclopentadienyl or C_5H_5; R = $-COCH_3$ (I), $-COCH_2SCH_3$ (II) and $-CO(CH_2)_3SCH_3$ (III)) in room temperature *n*-hexane solution were conducted in collaboration with Prof. Theodore J. Burkey and his group at the University of Memphis.[42] Self-closing ring reactions of these species are initiated by near-UV excitation (between 260 nm to 300 nm) of the metal-to-ligand charge transfer transition which leads to ejection of a single CO ligand and unpaired radical metal center in solution. They found that the quantum yields for I reacting with the sulfur atom of tetrahydrothiophene (THT) and self-ring closure between the Mn radical center and the Cp ligand sulfur atoms of II and III were $\phi = 0.82$, 1.0 and 0.82, respectively. Microsecond photoacoustic calorimetry measurements on these reactions were also unable to deduce mechanistic reasons for the differences in the observed quantum yields or whether transient species or structural effects at early times were controlling these reactions. Thus, it was decided that ultrafast transient infrared methods could be employed to directly monitor the early-time dynamics and mechanics of these intriguing molecular systems to try to extract reasons for the observed quantum yield differences.

Measurements of I with THT were conducted to test the capability of broadband IR for monitoring the disappearance of the parent species, identify any short-lived intermediates and determine the appearance time of the final product.[42] Since all parent and product species are stable, long-lived compounds, static FTIR spectra could first be used to identify and compare their time evolution from the transient IR results. In this case, bleaching bands of I (three IR-allowed fundamental CO-stretches) were observed at 2060 cm^{-1}, 1961 cm^{-1} and 1952 cm^{-1} and their amplitude did not change significantly during the entire observation time window. Two bands appear at 1907 cm^{-1} and 1969 cm^{-1} within the first 200 ps after excitation. These bands are attributed to the asymmetric and symmetric CO-stretch modes, respectively, of an *n*-hexane solvated (and vibrationally relaxed) transient intermediate. These transient absorption bands decay at the same rate ($2.3\ s^{-1} \pm 0.6 \times 10^{-6}\ s^{-1}$) as the appearance of the stable I-THT product bands at 1946 cm^{-1} and 1885 cm^{-1}. Thus, it is possible to distinguish transiently solvated dicarbonyls from the stable (Acyl-Cp)$(CO)_2$Mn-THT product and that the fundamental reaction rate is much smaller than the estimated average diffusion limited bimolecular encounter rate of a few hundred picoseconds. In this case the barrier to reaction may be high enough and thus makes the transient species lifetime extremely long (ca. 435 ns). Under these circumstances, many thousands of collisions are required on average before reaction occurs (implying $\phi = 1.0$) or recombination with liberated CO molecules also competes with the THT reaction (producing the observed less than unity quantum yields).

Related measurements of internal ring-closure reactions of II and III were performed but different rates and transients were identified (see Fig. 4). The reaction of II showed that within 200 ps of UV excitation, nearly equal populations of *n*-hexane solvent species and internal six-membered ring-closed species were created. The solvated species were subsequently found to self-react with a time constant of approximately 35 ns, indicating that this species has a much lower reaction barrier than I and that ring-closure reaction dominates over potential geminate recombination with liberated CO species. This could explain the reason for the near unity quantum yield for this species. However, reaction of III produced similar spectral features and transients as for the acyl compound (I) reacting with THT described above. Within 200 ps of excitation, an estimated ratio of solvated to eight-membered ring-closed species was found to be 3:1 (i. e., the propensity at early times is to form solvated species over internal ring-closure) and conversion of the solvated species to final product takes ca. 263 ns.

Considering all of the above observations and measured rate constants, a consistent picture of the reaction mechanisms emerges. Species I and III must have high enough reaction barriers (and hence several hundred nanosecond transiently solvated lifetimes) that reaction with an electron-rich sulfur center competes with CO recombination. Perhaps this scenario permits about 20% of the radical species enough time to recombine with CO while the remaining activated species either react with THT or self ring close. Solvated species II on the other hand appears to have a much lower reaction barrier than I and III (and hence ten times smaller lifetime) such that ring-closure competes favorably over any CO recombination and the ring-closure reaction quantum yield approaches unity for

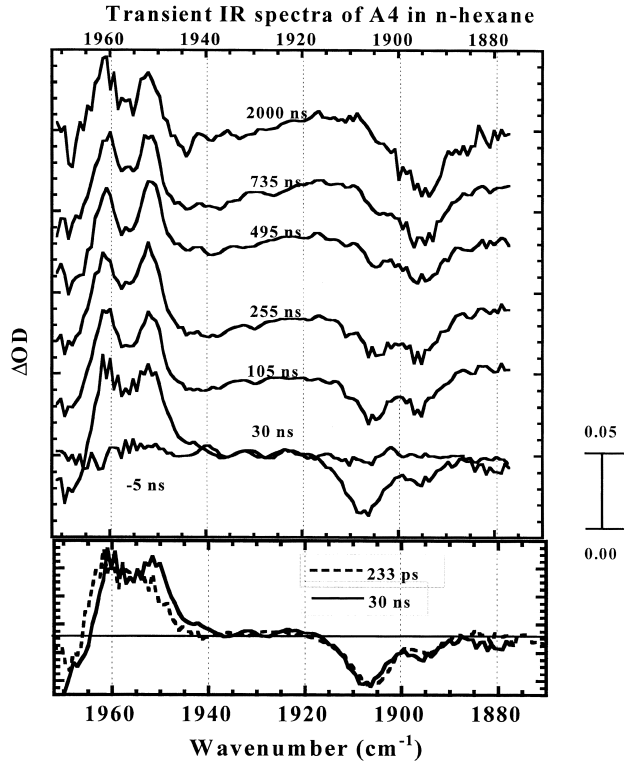

Fig. 4. Time-dependent transient IR spectra arising from the UV photolysis of the self ring-closing system $Mn(CO)_2$-Cp–$CO(CH_2)SH_3$ (Ⅲ) in *n*-hexane.

Ⅱ. Calculations of lowest energy conformations for Ⅱ and Ⅲ also suggest that Ⅱ spends about one-half of its time with the Mn radical center close to the sulfur atom while Ⅲ is approximately one-third in a reactive (close proximity) configuration for these atoms. This result is also consistent with the observed ratios of transiently solvated to ring-closed ratios measured at the earliest observation time delay (200 ps) discussed above. It should be added that the difference in reaction barrier heights may be controlled by steric factors (i. e., the propensity to form six versus eight membered ring compounds) and that the reaction enthalpy (ΔG) is dominated by entropic rather than enthalpic factors. Further molecular modeling and studies of these and other molecular self-closing reaction rates as a function of equilibrium system temperature may help uncover the source of these differences.

Terahertz Spectroscopy of Biomolecules. We are also exploring femtosecond methods for generating and detecting far-infrared (Terahertz or THz) broadband pulses in the 50 μm to 200 μm wavelength range (0.5 THz to 8 THz).[43] This spectroscopic approach is expected to allow time-dependent studies of low frequency torsional and rotational modes and dynamics of biological systems such as peptides, proteins and DNAs. The goal of our research is to apply these methods to making direct time-dependent dynamical measurements for collective motions associated with biological function. Towards this end, we obtained THz spectra of Calf-Thymus DNA (in polyethylene pellets and as a function of humidity), Bovine Serum albumin, and Collagen from 0.2 THz to 2 THz using a pulsed femtosecond apparatus.[43]

In order to access an appropriate THz frequency range where hydrogen-bonding and internal torsional modes dominate (3 THz to 10 THz or 100 cm^{-1} to 300 cm^{-1}), one would prefer to generate higher frequencies than are normally produced by biased antennas on LT-GaAs substrates (0.5 THz to 3 THz).[44] Semiconductor crystals (Ⅱ–Ⅳ and Ⅲ–Ⅴ) for broadband THz generators and electro-optic detectors (such as InP, GaAs, and ZnTe <110>) have been employed by others,[45] but these crystals were found to only typically work from 0.1 THz to 3 THz with 50 fs input pulses. We performed systematic transient femtosecond reflectivity measurements on the carrier dynamics of LT-GaAs and found that commercially grown material used for our linear dipole antenna structures produced a 1.6 ps lifetime. This result indicated a low carrier mobility and hence slow material response suggesting why we only observe usable detectable radiation below 3 THz. In-house grown 1 μm thick LT-GaAs on a GaAs substrate was produced by MBE with highly controlled deposition temperature (260 °C). This material exhibited a 350 fs carrier lifetime that should support much higher bandwidths when used as an antenna substrate. The most promising bandwidth conditions were found for high purity GaP <110> crystals (having internal optical phonon absorption at 11 THz). We were able to detect radiation out to 8 THz when 150 μm thick crystals of high transmission were employed (see Fig. 5). The high degree of variability and THz transmission of crystals obtained from various vendors implied that subtle manufacturing conditions (e. g., impurities, post heat treatment annealing, metallic microdroplet precipitation,

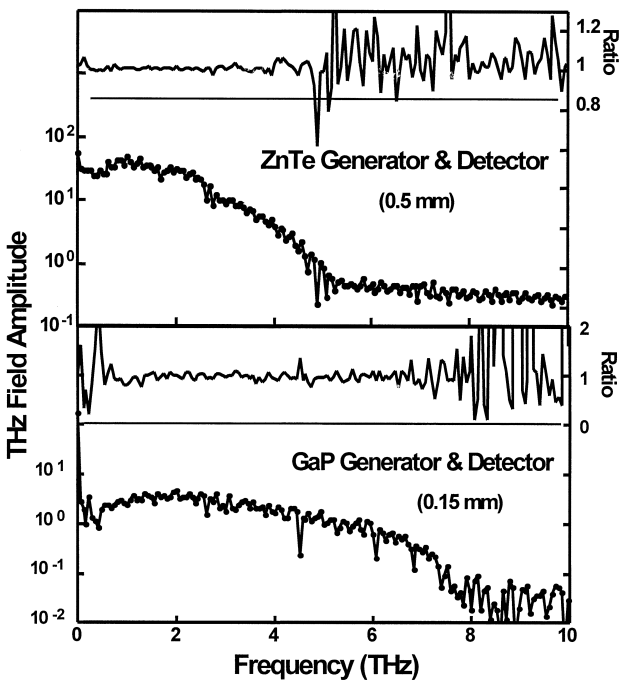

Fig. 5. Observed terahertz output power spectra for ZnTe and GaP generator and detector crystal combinations. For 50 fs input pulses, we find usable spectral bandwidth to 4 THz with ZnTe versus 7 THz, with slight loss in power, using highly transmissive GaP crystals. The displayed ratio arises from dividing two successive 100 average scans of the instrument at 2 cm^{-1} resolution.

etc.) drastically affect crystal performance. We suggest that careful specification and testing of these materials is required to obtain the desired bandwidths for future time-resolved THz investigations.

Conclusions and Future Directions

A description of broadband ultrafast infrared pulse generation and multi-channel CCD and IR focal plane detection methods has been reviewed. A few poignant examples of how these techniques can be used to extract photochemical reaction and electron transfer mechanisms, and to control vibrational excitation in complex systems were also described. The authors hope that more advanced measurements of chemical, material and biochemical systems will be made with higher time and spectral resolution using multi-channel infrared detectors as they become available to the scientific research community.

Extensions of these concepts to the study of low frequency hydrogen-bond stretches and cooperative librational motions of biopolymers in the condensed-phase and broadband surface sum-frequency spectroscopy[46] may now be explored. Novel broadband far-infrared generation and detection techniques are being used to obtain high-resolution spectra in the 0.5 THz to 10 THz frequency range of DNA and protein films and pressed pellets. It remains to be seen if intermolecular hydrogen-bond dynamics and functionally important biomolecular structural re-arrangements can be identified using time-resolved THz spectroscopy. However, detailed spectroscopic investigations in this region of the spectrum may become an important venue for future broadband transient spectroscopy of complex biological systems.

The authors are indebted to the hard work and focussed experimental efforts of many of our colleagues without whom this research would never have been possible. These include current NIST/NRC postdoctoral associate Dr. Larry Iwaki and Dr. Alan L. Migdall of the NIST Optical Technology Division, Prof. Theodore J. Burkey (Department of Chemistry, The University of Memphis, Memphis, TN, Dr. Joseph S. Melinger (Condensed Matter and Radiation Sciences Division, Naval Research Laboratory, Washington, DC) and former NIST/NRC postdoctoral research associates Drs. Valeria D. Kleiman, Andrea G. Markelz, David A. McWhorter, Steven Arrivo, Tom Dougherty (who passed away in 1997), Tandy Grubbs, and colleague Dr. Michael George (U. Nottingham, UK). We are also indebted to Dr. John Stephenson, of the NIST Laser Applications Group, for his support of this research and valuable scientific discussions. Research funding for most of this work was provided by internal NIST STRS support and the NIST Advanced Technology Program.

Glossary of Abbreviations

APCE — Absorbed Photon to Current Efficiency
CCD — Charge Coupled Device
DCM — 4-(Dicyanomethylene)-2-methyl-6-(*p*-dimethylaminostyryl)-4H-pyran (laser dye)
DNA — Deoxyribonucleic Acid
FROG — Frequency Resolved Optical Gating
FWHM — Full Width at Half Maximum
IR — Infrared
IRFPA — Infrared Focal Plane Array
LN2 — Liquid Nitrogen
LT-GaAs — Low Temperature grown Gallium Arsenide
NIST — National Institute of Standards & Technology
NRC — National Research Council
OPA — Optical Parametric Amplifier
QE — Quantum Efficiency
SHG — Second Harmonic Generation
STRS — Science and Technology Research Support
TE — Thermoelectric
THz — Terahertz
THT — Tetrahydrothiaphene
UV — Ultraviolet
vis — Visible
YAG — Yttrium Aluminum Garnet

References

1 A. Laubereau and W. Kaiser, *Rev. Mod. Phys.*, **50**, 607 (1978).
2 C. A. Moore and L. S. Goldberg, *Optics Comm.*, **16**, 21 (1976).
3 A. Laubereau, S. F. Fischer, K. Spanner, and W. Kaiser, *Chem. Phys.*, **31**, 335 (1978).
4 J.-C. Diels and W. Rudolph, "Ultrashort Laser Pulse Phenomena," Academic Press, San Diego (1996).
5 "Ultrafast Phenomena XI," ed by T. Elsaesser, J. G. Fujimoto, D. A. Wiersma and W. Zinth, Springer-Verlag, Berlin (1998).
6 P. Hamm, M. Lim, and R. M. Hochstrasser, *J. Phys. Chem. B*, **102**, 6123 (1998).
7 E. J. Heilweil, M. P. Casassa, R. R. Cavanagh, and J. C. Stephenson, *J. Chem. Phys.*, **81**, 2856 (1984).
8 E. J. Heilweil, M. P. Casassa, R. R. Cavanagh, and J. C. Stephenson, *Ann. Rev. Phys., Chem.*, **40**, 143 (1989).
9 R. Laenen, C. Rauscher, and A. Laubereau, *Phys.Rev. Lett.*, **80**, 2622 (1998).
10 H.-K. Nienhuys, S. Woutersen, R. A. van Santen, and H. J. Bakker, *J. Chem. Phys.*, **111**, 1494 (1999).
11 E. J. Heilweil, *Chem. Phys. Lett.*, **129**, 48 (1986).
12 E. J. Heilweil, M. P. Casassa, R. R. Cavanagh, and J. C. Stephenson, *J. Chem. Phys.*, **82**, 5216 (1985).
13 W. T. Grubbs, T. P. Dougherty, and E. J. Heilweil, *Chem. Phys. Lett.*, **227**, 480 (1994).
14 T. P. Dougherty and E. J. Heilweil, *Chem. Phys. Lett.*, **227**, 19 (1994).
15 E. J. Heilweil, *Optics Lett.*, **14**, 551 (1989).
16 T. P. Dougherty and E. J. Heilweil , *Optics Lett.*, **19**, 129 (1994).
17 S. M. Arrivo, V. D. Kleiman, T. P. Dougherty, and E. J. Heilweil, *Optics Lett.*, **22**, 1488 (1997).
18 H. Yang , P. T. Snee, K. T. Kotz , C. K. Payne, H. Frei, and C. B. Harris CB, *J. Am. Chem. Soc.*, **121**, 9227 (1999).
19 P. Hamm, S. Wiemann, M. Zurek, and W. Zinth, "Ultrafast Phenomena IX," ed by P. F. Barbara, W. H. Knox, G. A. Mourou, and A. H. Zewail, Springer-Verlag, Berlin (1994) pp. 152–153.
20 J. D. Beckerle, R. R. Cavanagh, M. P. Casassa, E. J. Heilweil, and J. C. Stephenson, *J. Chem. Phys.*, **95**, 5403 (1991).
21 L. H. Kidder, I. W. Levin, E. N. Lewis, V. D. Kleiman, and E. J. Heilweil, *Optics Lett.*, **22**, 742 (1997).
22 T. A. Heimer and E. J. Heilweil, "Proceedings for Ultrafast

Phenomena XI," Springer-Verlag, Berlin (1998), pp. 505–507.
23 T. P. Dougherty, W. T. Grubbs, and E. J. Heilweil, *J. Phys. Chem.*, **98**, 9396 (1994).
24 C. Chudoba, E. T. J. Nibbering, and T. Elsaesser, "Ultrafast Phenomena XI," ed by T. Elsaesser, J. G. Fujimoto, D. A. Wiersma and W. Zinth, Springer-Verlag, Berlin (1998), pp. 535–537.
25 T. P. Dougherty and E. J. Heilweil, "Time-resolved Vibrational Spectroscopy VI," A. Lau, F. Siebert, and W. Werncke, eds. Berlin: Springer-Verlag, Proceedings in Physics Volume 74, Berlin (1994), pp. 136–140.
26 W. T. Grubbs, T. P. Dougherty, and E. J. Heilweil, *Chem. Phys. Lett.*, **227**, 480 (1994).
27 T. P. Dougherty and E. J. Heilweil, *J. Chem. Phys.*, **100**, 4006 (1994).
28 Certain commercial materials are identified in this paper in order to adequately specify the experimental procedure. In no case does such identification imply recommendation or endorsement by the National Institute of Standards and Technology, nor does it imply that the materials or equipment are necessarily the best available for the purpose.
29 T. A. Heimer and E. J. Heilweil, *J. Phys. Chem. B*, **101**, 10990 (1998).
30 M. K. Nazeerudin, P. Liska, J. Moser, N. Vlachopoulos, and M. Gratzel, *Helvetica Chim. Acta.*, **73**, 1788 (1990).
31 T. Hannappel, B. Burfeindt, W. Storck, and F. J. Willig, *J. Phys. Chem. B*, **101**, 6799 (1997).
32 R. J. Ellington, J. B. Asbury, S. Ferrene, H. N. Ghosh, J. R. Sprague, T. Lian, and A. J. Nozik, *J. Phys. Chem. B*, **102**, 6455 (1998).
33 R. Argazzi, C. A. Bignozzi, T. A. Heimer, F. N. Castellano, and G. J. Meyer, *Inorg. Chem.*, **33**, 5741 (1994).
34 T. A. Heimer (unpublished results).
35 V. D. Kleiman, S. M. Arrivo, J. S. Melinger, and E. J. Heilweil, "Special issue on Coherence in Chemical Dynamics," *Chem. Phys.*, **223**, 207 (1998).
36 J. S. Melinger, D. McMorrow, C. Hillegas, and W. S. Warren, *Phys. Rev. A*, **51**, 3366 (1995).
37 J. D. Beckerle, R. R. Cavanagh, M. P. Casassa, E. J. Heilweil, and J. C. Stephenson, *Chem. Phys.*, **160**, 487 (1992).
38 S. M. Arrivo, T. P. Dougherty, W. T. Grubbs, and E. J. Heilweil, *Chem. Phys. Lett.*, **235**, 247 (1995).
39 B. A. Richman, M. A. Krumbugel, and R. Trebino, *Optics Lett*, **22**, 721 (1997).
40 W.-K. Liu, B. Wu, and J.-M.Yuan, *Phys. Rev. Lett.*, **75**, 1292 (1995).
41 S. A. Trushin, K. Sugawara, and H. Takeo, *Chem. Phys.*, **203**, 267 (1996).
42 T. Jiao, Z. Pang, T. J. Burkey, R. F. Johnston, T. A. Heimer, V. D. Kleiman, and E. J. Heilweil, *J. Am. Chem. Soc.*, **121**, 4618 (1999).
43 A. G. Markelz, A. Roitberg, and E. J. Heilweil, *Chem Phys Lett.*, **320**, 42 (2000).
44 A. G. Markelz and E. J. Heilweil, *App. Phys. Lett.*, **72**, 2229 (1998).
45 Q. Wu and X.-C. Zhang, *Appl. Phys. Lett.*, **68**, 1604 (1996).
46 L. J. Richter, T. Petralli-Mallow, and J. C. Stephenson, *Optics Lett.*, **23**, 1594 (1998).

Todd A. Heimer is a research chemist in the Optical Technology Division of the Physics Laboratory at NIST in Gaithersburg, MD. He obtained his degree in Physical Chemistry with Prof. Gerald Meyer at the Johns Hopkins University in 1996. He then joined the Laser Applications Group, Optical Technology Division as a NRC postdoctoral associate. During 1991–1998, He was primarily involved in using pump–probe visible and infrared spectroscopy to measure interfacial electron transfer rates in dye-sensitized metal oxide electrodes for solar energy conversion. Research from 1998 to 2001 focused on infrared imaging for spectroscopy and time-resolved experiments. His current primary research interest is developing and constructing the new NIST Retroreflectance facility.

Edwin J. Heilweil is a research chemist in the Laser Applications Group, Optical Technology Division of the Physics Laboratory at NIST in Gaithersburg, MD. He obtained his degree in Chemical Physics with Prof. Robin Hochstrasser at the University of Pennsylvania in 1984 at which time he joined the Center for Chemical Physics as a NBS/NRC postdoctoral associate. In 1986 he became a staff member of the Molecular Spectroscopy Division which is now part of the NIST Optical Technology Division. He was primarily involved in measuring ultrafast vibrational energy dynamics and photochemistry in liquids and for adsorbates on solids during 1984–1994. His current primary research interests include developing novel ultrafast infrared laser measurement methods, applying multiplexed infrared array detector techniques for chemical imaging and spectroscopy, and to monitor energy transfer and chemical reaction dynamics of biomolecular species using far-infrared technology (THz) in solution and on surfaces. He is a member of the American Chemical Society, Optical Society of America and Sigma Xi.